Ultra-High Quality Factor Resonances in a Pinwheel-Shaped All-Dielectric Metasurface Based on Bound States in the Continuum

Yan Shi, Shilin Yu, Hao Li, Jiaojiao Xing, and Tonggang Zhao

***Abstract*—Combining with the bound states in the continuum (BICs) theory in all-dielectric metasurfaces has become an extensively used method to excite multiple high quality(Q) factor Fano resonances, which remarkably enhance the performance of structures to be applied to refractive index sensors. In this article, a novel silicon pinwheel-shaped all-dielectric metasurface in the near-infrared region is designed and numerically investigated. Two Fano resonances are excited in the original structures. After breaking the symmetry of the original structures in combination with the BIC theory, four sharp Fano resonances are excited and the maximum Q-factor exceeds 3.9×10^5 when $\delta = 10$ nm. With the asymmetric parameter $\delta = 80$ nm, multiple Fano resonances could be turned on and off by turning the polarization of the incident light, which performs excellent characteristics in optical switches. Both in the original structures and in the asymmetric state it offers outstanding sensing characteristics. Furthermore, with $\delta = 80$ nm and the polarization angle 90 degrees, the sensitivity and the figure of merit (FOM) could respectively reach up to 355 nm/RIU and 1375.97 RIU^{-1}. The designed structures may provide a way to enhance the performance of bio-chemical sensors, optical switches, and nonlinear optics.**

***Index Terms*—All-dielectric metasurface, bound states in the continuum, high Q-factors, optical sensing, optical switches.**

I. Introduction

FANO resonance is a resonance showing asymmetric spectral lineshape. Its resonant linear pattern cannot be described by the traditional Lorentz formula. The Fano resonance spectrum was discovered in 1935 by H. Beutler et al. and subsequently interpreted by U. Fano [1], [2], [3]. Q-factor is a crucial parameter to assess the performance of Fano resonance. At present, Fano resonance with a high Q-factor has been widely used in the field of optics, such as nonlinear optics [4], [5], high performance sensor [6], [7], [8], and laser [9], [10]. But the metal-based plasma nanostructures such as free electron oscillation causes large ohmic loss, which leads to wide resonant spectral lines. In contrast, dielectric micro-nano devices such as germanium, gallium arsenide and silicon with high refractive index can result in lower ohmic loss, and the light field is mainly confined inside the device, which is favorable to enhance the interaction between light and matter inside the material [11], [12]. Thereupon Fano resonances could reach up to much higher Q-factors in all-dielectric metasurfaces. Additionally, different from metal-based nanostructures that only support electric dipoles oscillation, all-dielectric metasurfaces import magnetic responses so as to be able to create conditions for tuning interference of electric dipoles, magnetic dipoles, and other multipoles [13], [14], [15]. All-dielectric metasurfaces also have lower manufacturing costs than metal-based nanostructures and it is expected to achieve large-scale integrated production. Based on the above characteristics, Fano resonance research based on all-dielectric metasurfaces is of great significance.

The optical refractive index sensor is a typical utilization of Fano resonance [16], [17]. A sensor is a detection device, which converts the measured information into electrical signals and other output forms in terms of particular regulations. The past decades have seen the development by leaps and bounds of optical sensors with high sensitivity and figure of merit (FOM) [18], [19], [20]. Metasurfaces are very suitable for being applied to sensors due to their tiny size and easy integration. In related researches, super high Q-factor and outstanding sensing performance have made all-dielectric metasurfaces receive considerable critical attention. As an illustration, in 2018, Zhang Yuebian's group designed and numerically analyzed a high Q-factor, high modulation depth, multiple Fano resonance device based on periodic asymmetric clusters of Si nanorods in the near-infrared regime [21]. Then the study by Wang Yulin et al. investigated ultra high-Q factor toroidal multipole (TD) resonances at terahertz frequencies in all-dielectric metasurface composed of an array of high-index tetramer clusters in 2021, which propose a fresh idea to develop ultrasensitive photonic sensor in the terahertz regime [22]. Recently, Wang Juan's team investigated silicon metasurfaces composed of crescent shaped meta-atoms, which can be exploited for sensing ultrathin layers of biomolecules in air and buffer solutions [23]. Not only that, but also lower fabrication costs and compatibility with CMOS processes make all-dielectric metasurface sensors more attractive.

Manuscript received 31 January 2023; revised 17 February 2023; accepted 21 February 2023. Date of publication 24 February 2023; date of current version 9 March 2023. This work was supported by the National Natural Science Foundation of China under Grant 61835002 and in part by the National Key Research and Development Program of China under Grant 2022YFF0707100. *(Corresponding author: Tonggang Zhao.)*

Yan Shi, Hao Li, Jiaojiao Xing, and Tonggang Zhao are with the Beijing Key Laboratory of Space-ground interconnection and convergence, Beijing University of Posts and Telecommunications, Beijing 100876, China, and also with the School of the Electronic and Engineering, Beijing University of Posts and Telecommunications, Beijing 100876, China (e-mail: synm7@bupt.edu.cn; lihao2019@bupt.edu.cn; jiaojxing@bupt.edu.cn; zhaotg@bupt.edu.cn).

Shilin Yu is with the Research Center on Vector Optical Fields, Institute of Optics and Electronics, Chinese Academy of Sciences, Chengdu 610209, China (e-mail: yusl1017@163.com).

Digital Object Identifier 10.1109/JPHOT.2023.3248660

In recent years, the bound states in the continuum (BICs) have become a popular research method to stimulate high Q-factor multiple Fano resonance. BIC is a localized wave that lies in the continuum of radiation states, yet remains perfectly localized [24], [25], [26]. This theory is applicable to a very large deal of fluctuation phenomena, so it can be implemented in many different fields of wave physics including acoustics, microwaves, and nanophotonics [27]. In optical structures, true BICs exist simply in ideal lossless infinite structures. Because the resonance is not coupled with free space radiation, its linewidth is zero so its Q-factor is infinite, which can achieve perfect confinement of energy [28]. By breaking the symmetry to construct radiation channels with the free space, such as oblique incidence or the introduction of symmetric breakage in the structures, the BIC mode can be converted into a quasi-BIC mode [29], [30]. Furthermore, the resonant wavelengths, Q-factors, linewidths, and so on can be modulated by tuning the asymmetry degree. Up to the present, researchers have proposed a variety of metamaterial structures to achieve quasi-BIC by breaking the symmetry [31], [32], [33]. For instance, Shiyu Li's group investigated the symmetry-protected BIC supported by metasurfaces composed of silicon nanodisks and demonstrated the excitation of quasi-BIC by adding or removing parts of the nanodisks from the edge in 2019 [34]. In 2022, our group proposed a permittivity-asymmetric all-dielectric metasurface, comprising high-index cuboid tetramer clusters with symmetric structural parameters, which supported an uncommon route to design dual-band polarization-insensitive TD quasi-BICs resonators and facilitates their applications in optic and photonic [35]. Lately, Shuyuan Xiao et al. demonstrated the all-dielectric metasurfaces composed of four silicon nanodisks, in which the high Q-factor resonance with strongly enhanced local fields lead to significant enhancement of the THG and fifth-harmonic generation (FHG) signals through the symmetry breaking [36]. The BIC theory provides an excellent idea for realizing multiple Fano and high Q-factors in all-dielectric metasurfaces.

In this article, a pinwheel-shaped all-dielectric metasurface with multiple Fano resonances is proposed. It consists of a pair of nanorods placed vertically in the center and four isosceles trapezoids symmetrically placed around the nanorods. Its maximum Q-factor can reach up to 3.9×10^5, the sensor sensitivity can reach 350 nm/RIU and the FOM value can reach 907.44 RIU^{-1}. We adopted the finite difference theory of time domain (FDTD) to derive the transmission spectra and electromagnetic (EM) field distributions of the designed structures and then decomposed the scattered field into the contributions of three basic electromagnetic sources to investigate the Fano resonance excitation at different positions more clearly. Changing the geometric parameters of the structures can adjust the wavelength of Fano resonances with the modulation depth maintaining nearly 100%. When the symmetry in the structures was broken by tuning the baseline of one of the four isosceles trapezoids, it converts the BIC mode to quasi-BIC mode and excites four high Q-factor Fano resonances. By calculating the inverse square law that the Q-factors and the degree of asymmetry satisfy, the transition process from the BIC mode to the quasi-BIC mode is verified. And the maximum Q-factor can reach up to 39126.1 when $\delta = 10$ nm. In the original structures, tuning the polarization direction of incident light makes the structure perform polarization-independent result from its central symmetry. But in the same case, seven Fano resonances could be turned on and off in the asymmetric structures, with the modulation depth of every peak nearly 100%. The sensor sensitivity and the FOM value can reach up to 355 nm/RIU and 1375.97 RIU^{-1} respectively, with the polarization angle is 90°. It provides an exciting opportunity to advance biochemical sensors, optical switches, and nonlinear optics.

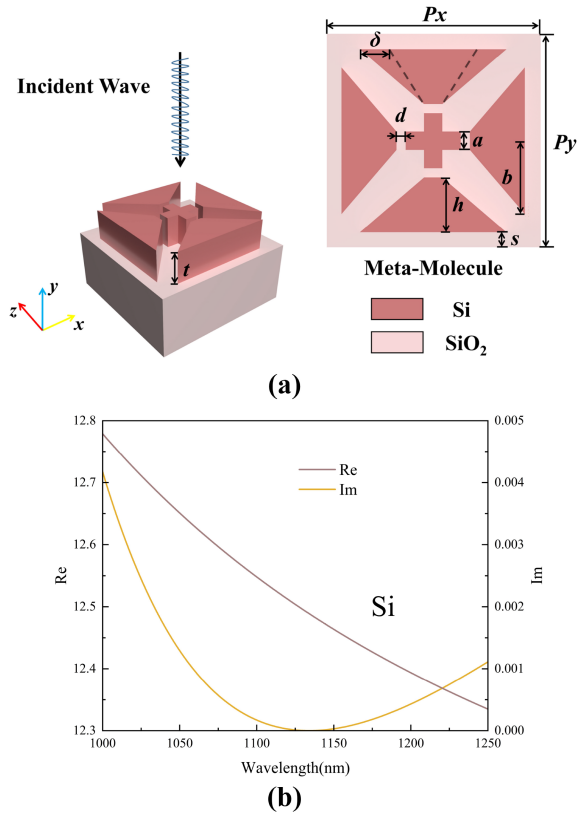

Fig. 1. (a) The designed Pinwheel-shaped all-dielectric metasurface consists of a pair of identical nanorods placed vertically in the center and four isosceles trapezoids symmetrically placed around the nanorods. The geometrical parameters are $a = 60$ nm, $b = 240$ nm, $h = 180$ nm, $d = 30$ nm, $Px = Py = P = 700$ nm, $s = 50$ nm, $t = 150$ nm. (b) The real and imaginary parts of the dielectric constant of the silicon in the experimental wave band.

II. Structures Description

The designed Pinwheel-shaped all-dielectric metasurface is shown in Fig. 1(a). It consists of a pair of identical nanorods placed vertically in the center and four isosceles trapezoids symmetrically placed around the nanorods. The structure is placed on a silica substrate and immersed in a liquid with the background refractive index $n = 1.33$. The structures are centrally symmetric. The silicon is amorphous. The dispersion properties of the materials refer to Palik' s optical manual, and the real and imaginary parts of the dielectric constant of the silicon in the experimental wave band are shown in Fig. 1(b) [37]. The plane wave electric field is incident perpendicular to the metasurface and polarized

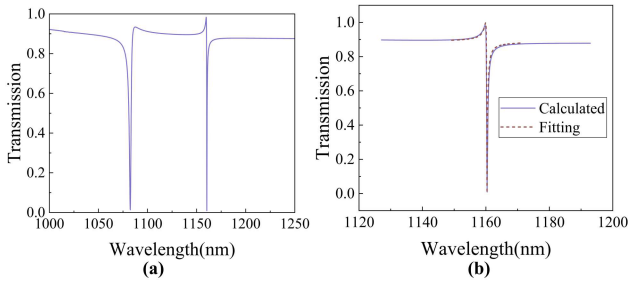

Fig. 2. (a) Transmission spectrum of the designed structures. (b) FDTD Simulation Results and Fitting Graphs at λ = 1160.4 nm. The brown dashed lines represent the result of the Fano formula fitting and the purple solid line represents the result of the FDTD calculation.

along the *x*-axis (polarization angle $\theta = 0°$). The nanorod has the width *a*, which is equal to the topline of the isosceles trapezoid, and the length *3a*. Half of the baseline of the isosceles trapezoid is *b*, and its height is *h*. The distance between nanorods and trapezoids is *d*. The period of the unit structure *Px* = *Py*. The thickness is *t*. And the distance from the baseline of the trapezoid to the boundary of the unit structures is *s*. The FDTD module of Ansys Lumerical Photonics Simulation & Design Software gets used for deriving the transmission spectra and electromagnetic (EM) field distributions of the proposed structures. Simulation work utilizes periodic boundary conditions in both the *x* and *y* directions, and in the *z* direction, a perfectly matched layer (PML) is utilized.

III. Stimulation and Multipoles Expansion

When *Px* = *Py* = 700 nm, *x* = *y* = 600 nm, *t* = 150 nm and *d* = 300 nm, the transmission curves of the metasurfaces are described in Fig. 2(a). Two sharp Fano profile curves appear at λ = 1082.4 nm and λ = 1160.4 nm, respectively. Q-factor is one of the significant parameters for measuring metasurface performance thus, the transmission spectra can be qualitatively analyzed using the Fano model. The formula is given by

$$T_{Fano} = \left| a_1 + ia_2 + \frac{b}{\omega - \omega_0 + i\gamma} \right|^2 \tag{1}$$

where a_1, a_2 and b are constant real numbers, γ is the overall damping loss, and ω_0 is the resonant central frequency [38]. $A = a_1 + ia_2$ can denote the continuous states and $B = b/(\omega - \omega_0 + i\gamma)$ can denote the discrete states. And the Q-factor can be expressed as:

$$Q_{rad} = \frac{\omega_0}{2\gamma} \tag{2}$$

Fig. 2(b) shows the fitting results at λ = 1160.4 nm. The fitting curve (brown dashed line) is definitely consistent with the simulation results (the purple line). It is calculated that the Q-factor reached 3117.99 at λ = 1160.4 nm. The scattered field can be decomposed into the contributions of three basic electromagnetic sources, namely electric multipoles, magnetic multipoles, and toroidal multipoles (TD). Electric multipoles include electric dipole (ED) and electric quadrupole (EQ), etc.

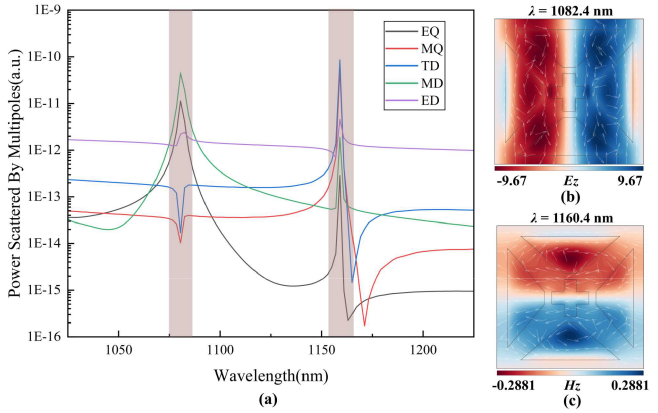

Fig. 3. (a) The radiating powers of various multipole moments in the original structures. (b) Electronic field distribution in the *x*-*y* plane at λ = 1082.4 nm. Arrows denote the direction of the magnetic field line. (c) Magnetic field distribution in the *x*-*y* plane at λ = 1160.4 nm. Arrows denote the direction of the electric field line.

Likewise, magnetic dipole (MD) and magnetic quadrupole (MQ) etc. are contained in magnetic multipoles. In the Cartesian coordinate system, the electric dipole moment $\boldsymbol{p}$ can be defined as:

$$\boldsymbol{p} = \frac{1}{i\omega} \int \boldsymbol{j} d^3 r \tag{3}$$

The magnetic dipole moment $\boldsymbol{m}$ can be defined as:

$$\boldsymbol{m} = \frac{1}{2c} \int (\boldsymbol{r} \times \boldsymbol{j})\, d^3 r \tag{4}$$

The toroidal dipole moment $\boldsymbol{T}$ can be defined as:

$$\boldsymbol{T} = \frac{1}{10c} \int \left[(\boldsymbol{r} \cdot \boldsymbol{j})\, \boldsymbol{r} - 2r^2 \boldsymbol{j} \right] d^3 r \tag{5}$$

The electric quadrupole $\boldsymbol{Q}^{(e)}_{\boldsymbol{\alpha\beta}}$ can be defined as:

$$\boldsymbol{Q}^{(e)}_{\boldsymbol{\alpha\beta}} = \frac{1}{i2\omega} \int \left[r_\alpha j_\beta + r_\beta j_\alpha - \frac{2}{3} (\boldsymbol{r} \cdot \boldsymbol{j})\, \delta_{\alpha,\beta} \right] d^3 r \tag{6}$$

And the magnetic quadrupole $\boldsymbol{Q}^{(m)}_{\boldsymbol{\alpha\beta}}$ can be defined as:

$$\boldsymbol{Q}^{(m)}_{\boldsymbol{\alpha\beta}} = \frac{1}{3c} \int \left[(\boldsymbol{r} \times \boldsymbol{j})_\alpha r_\beta + (\boldsymbol{r} \times \boldsymbol{j})_\beta r_\alpha \right] d^3 r \tag{7}$$

where c represents the speed of light in a vacuum, ω is the angular frequency, $\boldsymbol{r}$ represents the spatial position vector, α, β = *x*, *y*, *z*. $\boldsymbol{j}$ is the current density [31]. To explain this Fano resonance of the designed all-dielectric metasurface more clearly, the contributions of multipoles in forming the resonant responses are evaluated in Fig. 3(a), and the electromagnetic (EM) fields at the corresponding resonant wavelengths are described in Fig. 3(b) and (c), respectively. Fig. 3(a) calculated the radiating powers of various multipole moments. The strongest response should be MD at λ = 1082.4 nm and TD at λ = 1160.4 nm. As shown in Fig. 3(b) and (c) the electromagnetic field distribution corresponds to the strongest dipole response. At λ = 1082.4 nm, two reversed loops in the *x*-*y* plane formed by the magnetic field and a vortex flowing anticlockwise in the *x*-*z* plane formed

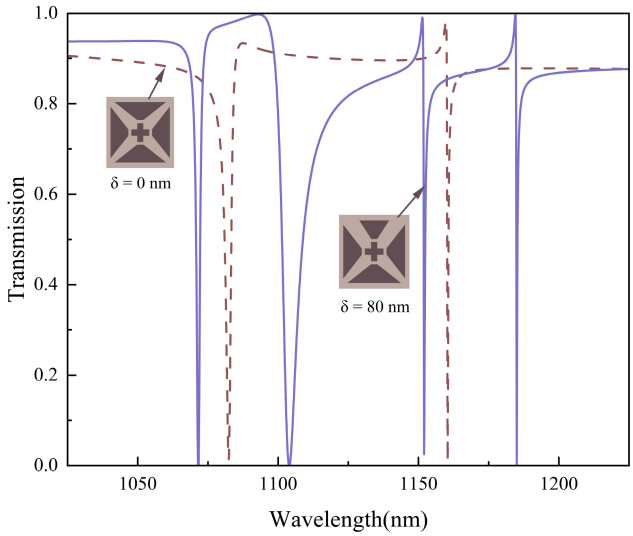

Fig. 4. Transmission spectra contrast of the original structures and the asymmetric structures. The brown dashed line depicts the spectrum at $\delta = 0$ nm and the purple solid line depicts the spectrum at $\delta = 80$ nm.

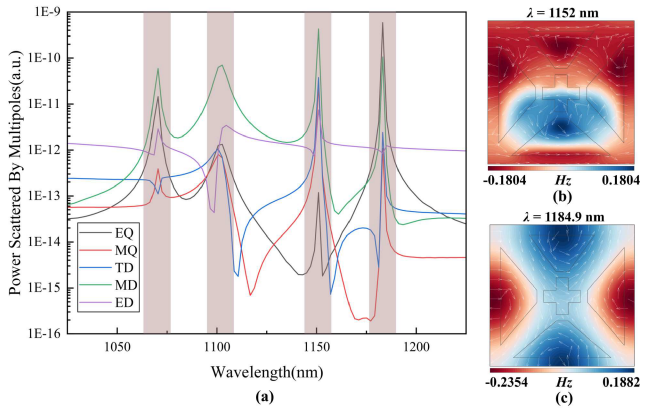

Fig. 5. (a) The radiating powers of various multipole moments in the asymmetric structures. (b) Magnetic field distribution in the x-y plane at $\lambda = 1152$ nm. (c) Magnetic field distribution in the x-y plane at $\lambda = 1184.9$ nm. Arrows denote the direction of the electric field line.

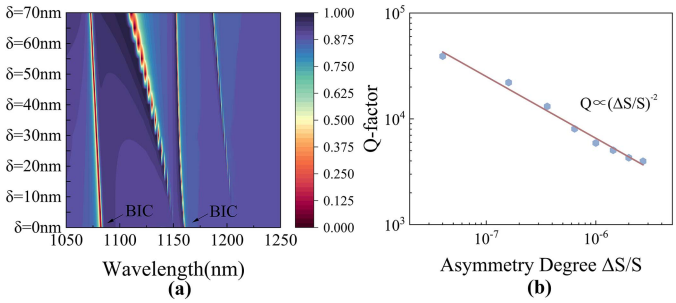

Fig. 6. (a) Comparison of transmission spectra at different asymmetry degrees δ. (b) The quantity relation between the Q-factor and asymmetry degree meets $Q_{rad} \propto \alpha^{-2}$ at $\lambda = 1184.9$ nm.

by the electric field, demonstrating that the resonant mode at this wavelength is MD along the y-negative direction. At $\lambda = 1160.4$ nm, the electric field forms two reversed loops in the x-y plane and the magnetic field forms a loop clockwise in the y-z plane, indicating that this is a TD resonance pattern along the x-negative direction.

To realize multiple Fano and high Q-factor all-dielectric metasurfaces, the symmetry of the original structures is broken to construct radiation channels with the free space. It converts symmetry-protected BIC into quasi-BIC. The asymmetric parameter δ is equal to the variation of the parameter b of the top trapezoid. As shown in Fig. 4, when $\delta = 80$ nm, at $\lambda = 1071.5$ nm, and $\lambda = 1152$ nm, the transmission spectrum has a blue shift because of the breaking symmetry, respectively. At the same time, two new Fano profile curves arise at $\lambda = 1103.8$ nm and $\lambda = 1184.9$ nm. The contributions of multipoles in forming the resonant responses are evaluated in Fig. 5(a), and the EM fields at the corresponding resonant wavelengths are drawn in Fig. 5(b) and (c). In Fig. 5(a), the strongest response should be MD at $\lambda = 1152$ nm and EQ at $\lambda = 1184.9$ nm. As shown in Fig. 5(b), at $\lambda = 1152$ nm, two reversed loops in the x-y plane formed by the magnetic field and a vortex flowing anticlockwise in the y-z plane formed by the electric field, demonstrating that the resonant mode at this wavelength is MD along the z-negative direction. Differently, in accordance with the electric field vector distributions at 1184.9 nm in Fig. 5(c), indicating an EQ resonance at this wavelength.

The Q-factors, resonant wavelengths, line widths and so on can be modulated by tuning the asymmetry degree. As shown in Fig. 6(a), when the structure is symmetrical, the resonance mode is BIC and the Q-factor tends to be infinite. Whereas, as δ increases, two new asymmetric resonance profiles emerge near $\lambda = 1125$ nm and $\lambda = 1190$ nm, and the transmission spectrum has a blue shift. Furthermore, the bigger the δ, the wider the line widths and the smaller the Q-factors. It is because breaking the symmetry constructs radiation channels with the free space. The bigger the δ, the wider the radiation channel, which means that more energy is lost by the radiation, and therefore, the less the Q-factors. When $\delta = 10$ nm, the Q-factor is 39126.1 at $\lambda = 1184.9$ nm. In addition, it can be seen that in the quasi-BICs, the performance of the structures is very sensitive to the changes of asymmetry degree. In Table I the Q-factors and the asymmetry degree $\alpha = \Delta S/S$ of $\delta = 10 - 80$ nm are calculated, where ΔS is the reduced area of the altered trapezium and S is the area of one original trapezium. The asymmetry degree α and the Q-factors satisfy following formula under the quasi-BIC resonance state:

TABLE I
THE Q-FACTOR AND THE ASYMMETRY DEGREE $\alpha = \Delta S/S$ OF $\delta = 10$-80 NM

δ(nm)	10	20	30	40	50	60	70	80
Q-factor	39126.1	22053.2	13112.8	8045.1	5907.6	5049.4	4291.3	3975
(ΔS/S)^(-2)	4.00E-08	1.60E-07	3.60E-07	6.40E-07	1.00E-06	1.44E-06	2.00E-06	2.70E-06

$$Q_{rad} = \frac{A}{2k_0}|p_0|^{-2}\left(\frac{\Delta S}{S}\right)^{-2} \tag{8}$$

where A represents the surface area of a meta-molecule, k_0 is the incident plane wave vector, and in our proposed structures,

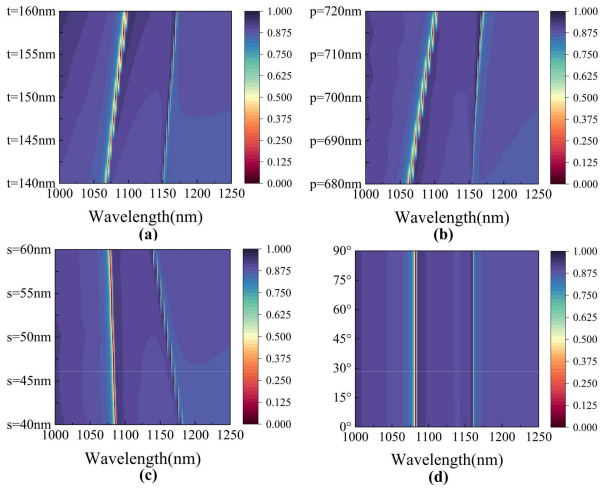

Fig. 7. Changes in the transmission spectra caused by adjusting different geometric parameters. (a) Thickness t of the designed metasurface is from 140 nm to 160 nm. (b) Period p of the designed metasurface is from 680 nm to 720 nm. (c) Distance from the baseline of the trapezoid to the boundary of the unit structures s is from 40 nm to 60 nm. (d) The transmission spectrum remains the same when the polarization direction changes.

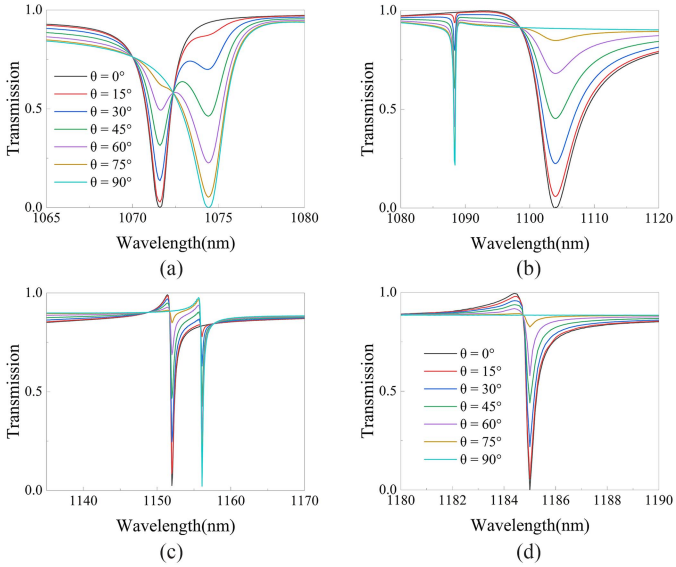

Fig. 8. Seven Fano resonances can be turned on and off by turning the polarization angle θ of incident light when $\delta = 80$ nm.

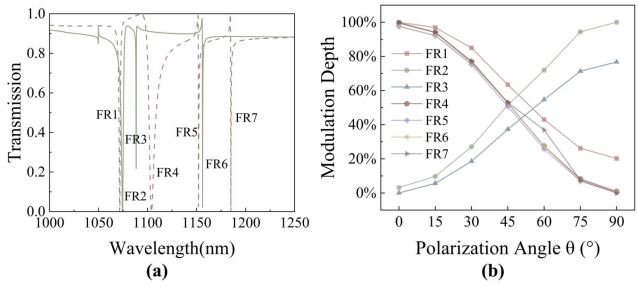

Fig. 9. (a) Transmission spectra contrast of the asymmetric structures with the polarization angle θ of incident light is 0° and 90°, respectively. The brown dashed line depicts the spectrum with $\theta = 0°$ and the green solid line depicts the spectrum with $\theta = 90°$. (b) The variation of modulation depths with the polarization angle from 0° to 90° at every Fano resonant wavelength.

p_0 is the ED moment in the bottom half of the nanocube [34]. Namely, the asymmetry degree α and the Q-factor satisfy the following relationship $Q_{rad}^{\propto\alpha^{-2}}$. In Fig. 6(b), the quantity relation between Q-factors and asymmetry degree meets $Q_{rad}^{\propto\alpha^{-2}}$ at $\lambda =$ 1184.9 nm is illuminated by calculating. It also proves that two new Fano resonances are excited by breaking the symmetry and achieving quasi-BIC.

IV. Parameters Adjustment and Polarization Analysis

To investigate the effect of the geometric independence of the structures on the characteristics of the designed metasurfaces, the thickness t, the period of the structures p, and the distance between nanorods and trapezoids s are adjusted, respectively. The other parameters remain the same as the structures in Fig. 2. The results are obtained through simulation. As shown in Fig. 7(a) and (b), increasing both the period p and the thickness t occurred significant redshifts in the transmission spectra at all two resonant wavelengths. Conversely, as shown in Fig. 7(c), when distance s gradually increases, the resonant wavelengths have a blue shift and its line width increases, accordingly the corresponding Q-factor decreases. Therefore, the resonant wavelengths of the proposed structure can be adjusted by optimizing the geometric parameters of the structure.

In order to study the application potential of the structures in optical switching, the effects of changing the polarization direction of the light source of the designed metasurfaces are discussed. As shown in Fig. 7(d), it is notable that when the angle θ increases from 0° to 90° and the other parameters are the same as the structures in Fig. 2, the transmission spectra remain the same. More specifically, the metasurfaces perform polarization-independent. This occurs as a result of the central symmetry of the structures in the x-y plane. After breaking the symmetry, the metasurfaces achieve quasi-BIC mode and are no longer centrally symmetrical. The structures exhibit a highly sensitive to changing the polarization angle of incident light. As shown in Fig. 8, with the asymmetric parameter $\delta = 80$ nm, seven Fano resonances at $\lambda = 1071.6$ nm, 1074.4 nm, 1088.4 nm, 1104.1 nm, 1152 nm, 1156.1 nm, and 1184.9 nm can be turned on and off by tuning the polarization angle of the incident light. These Fano profiles are numbered FR1-FR7. Fig. 9(a) shows the transmission spectra when $\theta = 0°$ and $\theta = 90°$, respectively. Table II calculated the modulation depth of each Fano profile when the polarization angle of the incident light increased from

TABLE II
The Modulation Depth of Each Fano Profile When the Polarization Angle of Incident Light Increases From 0° to 90°

	FR1	FR2	FR3	FR4	FR5	FR6	FR7
0°	100.00%	3.16%	0.01%	99.46%	97.47%	97.76%	99.80%
15°	96.90%	9.73%	5.65%	94.04%	92.14%	92.24%	94.08%
30°	84.96%	27.07%	18.54%	76.91%	75.26%	76.20%	77.04%
45°	63.40%	51.47%	37.31%	52.66%	50.74%	52.82%	53.00%
60°	43.02%	71.93%	54.72%	27.44%	25.78%	27.39%	36.90%
75°	26.19%	94.41%	71.31%	8.24%	6.90%	7.24%	7.50%
90°	20.21%	100.00%	76.74%	0.91%	0.22%	0.50%	0.00%

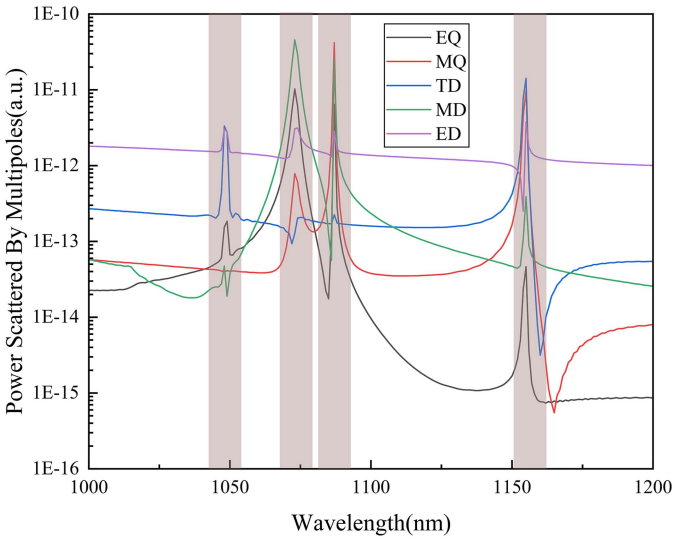

Fig. 10. The radiating powers of various multipole moments in the asymmetric structures with the polarization angle is 90°.

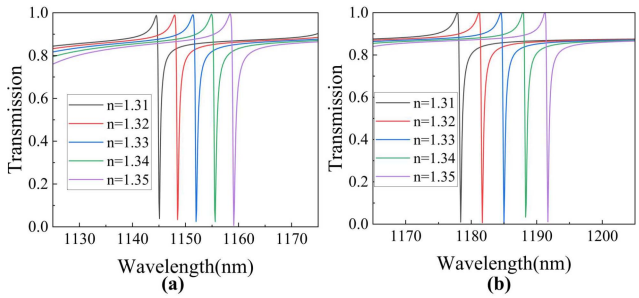

Fig. 11. (a) The transmission spectral shift at $\lambda = 1152$ nm as the environmental refractive index increases from 1.31 to 1.35. (b) The transmission spectral shift at $\lambda = 1184.9$ nm as the environmental refractive index increases from 1.31 to 1.35.

0° to 90°. It is intuitively that with the polarization angle from 0° to 90°, the modulation depths of FR1, FR4, FR5, FR6, and FR7 gradually rise, meanwhile the modulation depths of FR2 and FR3 are on downward trends. Moreover, the modulation depths of the transmission spectral line of FR2, FR4, FR5, FR6, and FR7 are close to 100%. The proposed all-dielectric metasurfaces can be widely applied to high performance optical switches. Consistent with the previous, As can be seen in Fig. 10, the radiating powers of various multipole moments are also calculated. The strongest response should be MQ at $\lambda = 1088.4$ nm and TD at $\lambda = 1156.1$ nm.

V. Sensing Application

To investigate the application potential of designed metasurfaces in terms of sensors, the impact of changes in the surrounding environment on the metasurfaces is discussed. Fig. 11(a) and (b) respectively demonstrate the transmission spectral shifts at $\lambda = 1152$ nm and $\lambda = 1184.9$ nm in the asymmetric structures. As the environmental refractive index increases from 1.31 to 1.35, the transmission spectra manifest redshifts significantly,

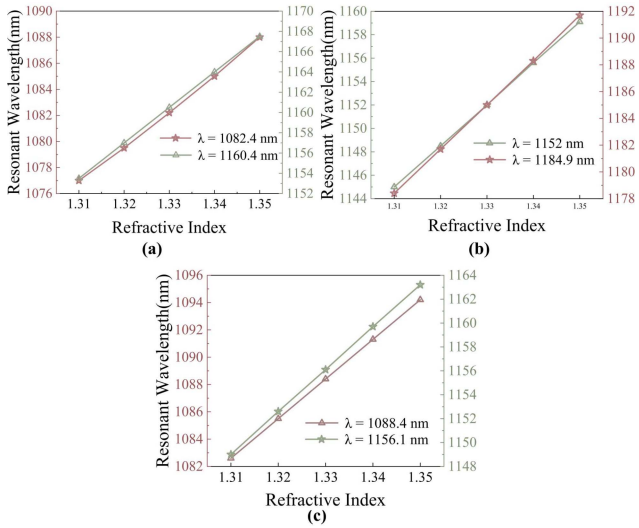

Fig. 12. (a) The resonant wavelength with different refractive indexes in original structures at $\lambda = 1082.2$ nm and 1160.5 nm. (b) The resonant wavelength with different refractive indexes in asymmetric structures at $\lambda = 1152$ nm and 1184.9 nm. (c) The resonant wavelength with different refractive indexes in asymmetric structures with $\theta = 90°$ at $\lambda = 1088.4$ nm and 1156.1 nm.

TABLE III
Sensitivity *S* and the Figure of Merit in Different Structures

Structures	The Original Structures		The Asymmetric Structures(θ = 0°)		The Asymmetric Structures(θ = 90°)	
Resonant Wavelength(nm)	1082.2	1160.5	1152	1184.9	1088.4	1156.1
Sensitivity(nm/RIU)	275	350	282	266	290	355
Δλ(nm)	3.4	0.386	0.416	0.298	0.277	0.258
the Figure of Merit(RIU^{-1})	80.9	907.44	677.88	892.62	1043.93	1375.97

while the Q-factor had little alteration. Sensitivity S is calculated from the ratio of the variation of resonant wavelength to the variation of refractive index. Fig. 12(a)–(c) respectively yield the resonant wavelength with different refractive indexes in different structures. The FOM value is a measure of sensor performance and the formula is as follows:

$$FOM = \frac{S\,(nm/RIU)}{\Delta\lambda\,(nm)} \tag{9}$$

where $\Delta\lambda$ is the line width of Fano resonance [12]. Table III shows the fitting result sensitivity S from Fig. 12(a)–(c) and the figure of merit (FOM). The sensitivity and FOM values of the proposed metasurfaces can reach up to 355 nm/RIU and 1375.97 RIU^{-1}, respectively. The designed all-dielectric metasurfaces can be widely applied to high-performance bio-chemical sensors.

VI. Conclusion

In conclusion, we proposed and numerically investigated novel all-dielectric metasurfaces and realize multiple Fano resonances with high Q-factors. The Q-factor can reach up to 39126.1 when asymmetry parameter $\delta = 10$ nm. The structures

exhibit polarization-independence because of their central symmetry. After breaking the symmetry, it can achieve at least seven Fano resonances, which can be turned on and off by tuning the polarization angle of the incident light and has an ultra-high modulation depth. The maximum sensitivity can reach up to 355 nm/RIU and the maximum FOM value can reach 1375.97 RIU^{-1}. The designed structures are expected to achieve potential applications in the fields of biochemical sensors, optical switches, and nonlinear optics because of their multi-Fano, high Q-factors, high FOM values, and high modulation depths.

REFERENCES

[1] H. Beutler, "Über absorptionsserien von argon, krypton und xenon zu termen zwischen den beiden ionisierungsgrenzen $^2P^0{}_{3/2}$ und $^2P^0{}_{1/2}$," *Zeitschrift Physik*, vol. 93, pp. 177–196, 1935.

[2] Y. S. Joe, A. M. Satanin, and C. S. Kim, "Classical analogy of Fano resonances," *Physica Scripta*, vol. 74, pp. 259–266, 2006.

[3] U. Fano, "Effects of configuration interaction on intensities and phase shifts," *Phys. Rev.*, vol. 124, pp. 1866–1878, 1961.

[4] A. Krasnok, M. Tymchenko, and A. Alù, "Nonlinear metasurfaces: A paradigm shift in nonlinear optics," *Mater. Today*, vol. 21, pp. 8–21, 2018.

[5] M. Kroner et al., "The nonlinear Fano effect," *Nature*, vol. 451, pp. 311–314, 2008.

[6] A. Ahmadivand et al., "Rapid detection of infectious envelope proteins by magnetoplasmonic toroidal metasensors," *ACS Sensors*, vol. 2, pp. 1359–1368, 2017.

[7] C. Wu et al., "Fano-resonant asymmetric metamaterials for ultrasensitive spectroscopy and identification of molecular monolayers," *Nature Mater.*, vol. 11, pp. 69–75, 2011.

[8] Z. Shen and M. Du, "High-performance refractive index sensing system based on multiple Fano resonances in polarization-insensitive metasurface with nanorings," *Opt. Exp.*, vol. 29, pp. 28287–28296, 2021.

[9] S. Kim et al., "High-Q metallic Fano metamaterial for highly efficient Cerenkov lasing," *Adv. Opt. Mater.*, vol. 6, 2018, Art. no. 1800041.

[10] H. Wang, R. Xu, J. Zhang, W. Zhou, and D. Shen, "Ultranarrow filter based on Fano resonance in a single cylindrical microresonator for single-longitudinal-mode fiber lasers," *Opt. Exp.*, vol. 27, pp. 22717–22726, 2019.

[11] W. X. Lim, M. Manjappa, P. Pitchappa, and R. Singh, "Shaping high-Q planar Fano resonant metamaterials toward futuristic technologies," *Adv. Opt. Mater.*, vol. 6, no. 19, 2018, Art. no. 1800502.

[12] H. Li, S. Yu, L. Yang, and T. Zhao, "High Q-factor multi-Fano resonances in all-dielectric double square hollow metamaterials," *Opt. Laser Technol.*, vol. 140, 2021, Art. no. 107072.

[13] M. Xu et al., "Emerging long-range order from a freeform disordered metasurface," *Adv. Mater.*, vol. 34, no. 12, 2022, Art. no. 2108709.

[14] R. Alaee, C. Rockstuhl, and I. Fernandez-Corbaton, "Exact multipolar decompositions with applications in nanophotonics," *Adv. Opt. Mater.*, vol. 7, no. 1, 2019, Art. no. 1800783.

[15] N. Papasimakis, V. A. Fedotov, V. Savinov, T. A. Raybould, and N. I. Zheludev, "Electromagnetic toroidal excitations in matter and free space," *Nature Mater.*, vol. 15, pp. 263–271, 2016.

[16] A. E. Cetin and H. Altug, "Fano resonant ring/disk plasmonic nanocavities on conducting substrates for advanced biosensing," *ACS Nano*, vol. 6, pp. 9989–9995, 2012.

[17] A. B. Khanikaev, C. Wu, and G. Shvets, "Fano-resonant metamaterials and their applications," *Nanophotonics*, vol. 2 pp. 247–264, 2013.

[18] J. B. Lassiter et al., "Fano resonances in plasmonic nanoclusters: Geometrical and chemical tunability," *Nano Lett.*, vol. 10, pp. 3184–3189, 2010.

[19] S. M. A. Sufian Sunny, T. Ahmed, S. M. Hiam, and A. K. Paul, "Highly sensitive externally metal coated plasmonic refractive index sensor based on photonic crystal fiber," *Optik*, vol. 243, 2021, Art. no. 167482.

[20] A. I. Kuznetsov, A. E. Miroshnichenko, and M. L. Brongersma, Y. S. Kivshar, and B. Luk'yanchuk, "Optically resonant dielectric nanostructures," *Science*, vol. 354, no. 6314, 2016, Art. no. aag2472.

[21] Y. Zhang et al., "High-quality-factor multiple Fano resonances for refractive index sensing," *Opt. Lett.*, vol. 43, pp. 1842–1845, 2018.

[22] Y. Wang, Z. Han, Y. Du, and J. Qin, "Ultrasensitive terahertz sensing with high-Q toroidal dipole resonance governed by bound states in the continuum in all-dielectric metasurface," *Nanophotonics*, vol. 10, pp. 1295–1307, 2021.

[23] J. Wang, J. Kühne, T. Karamanos, C. Rockstuhl, S. A. Maier, and A. Tittl, "All-dielectric crescent metasurface sensor driven by bound states in the continuum," *Adv. Funct. Mater.*, vol. 31, no. 46, 2021, Art. no. 2104652.

[24] C. W. Hsu, B. Zhen, A. D. Stone, J. D. Joannopoulos, and M. Soljačić, "Bound states in the continuum," *Nature Rev. Mater.*, vol. 1, no. 19, pp. 1–3, 2016.

[25] D. C. Marinica, A. G. Borisov, and S. V. Shabanov, "Bound states in the continuum in photonics," *Phys. Rev. Lett.*, vol. 100, 2008, Art. no. 183902.

[26] M. Zhang and X. Zhang, "Ultrasensitive optical absorption in graphene based on bound states in the continuum," *Sci. Rep.*, vol. 5, 2015, Art. no. 8266.

[27] A. Kodigala, T. Lepetit, Q. Gu, B. Bahari, Y. Fainman, and B. Kante, "Lasing action from photonic bound states in continuum," *Nature*, vol. 541, pp. 196–199, 2017.

[28] D. N. Maksimov, V. S. Gerasimov, S. Romano, and S. P. Polyutov, "Refractive index sensing with optical bound states in the continuum," *Opt. Exp.*, vol. 28, pp. 38907–38916, 2020.

[29] X. Liu et al., "Terahertz metasurfaces based on bound states in the continuum (BIC) for high-sensitivity refractive index sensing," *Optik*, vol. 261, 2022, Art. no. 169248.

[30] K. Koshelev, S. Lepeshov, M. Liu, A. Bogdanov, and Y. Kivshar, "Asymmetric metasurfaces with high-Q resonances governed by bound states in the continuum," *Phys. Rev. Lett.*, vol. 121, 2018, Art. no. 193903.

[31] L. Yang, S. Yu, H. Li, and T. Zhao, "Multiple Fano resonances excitation on all-dielectric nanohole arrays metasurfaces," *Opt. Exp.*, vol. 29, pp. 14905–14916, 2021.

[32] M. Li, Q. Ma, A. Luo, and W. Hong, "Multiple toroidal dipole symmetry-protected bound states in the continuum in all-dielectric metasurfaces," *Opt. Laser Technol.*, vol. 154, 2022, Art. no. 108252.

[33] S. Yu, H. Li, Y. Wang, Z. Gao, T. Zhao, and J. Yu, "Multiple Fano resonance excitation of all-dielectric nanoholes cuboid arrays in near infrared region," *Results Phys.*, vol. 28, 2021, Art. no. 104569.

[34] S. Li, C. Zhou, T. Liu, and S. Xiao, "Symmetry-protected bound states in the continuum supported by all-dielectric metasurfaces," *Phys. Rev. A*, vol. 100, no. 6, 2019, Art. no. 063803.

[35] S. Yu et al., "Dual-band polarization-insensitive toroidal dipole quasi-bound states in the continuum in a permittivity-asymmetric all-dielectric meta-surface," *Opt. Exp.*, vol. 30, pp. 4084–4095, 2022.

[36] S. Xiao, M. Qin, J. Duan, and T. Liu, "Robust enhancement of high-harmonic generation from all-dielectric metasurfaces enabled by polarization-insensitive bound states in the continuum," *Opt. Exp.*, vol. 30, pp. 32590–32599, 2022.

[37] E. D. Palik, *Handbook of Optical Constants of Solids*. New York, NY, USA: Academic , 1997.

[38] Y. Yang, I. I. Kravchenko, D. P. Briggs, and J. Valentine, "All-dielectric metasurface analogue of electromagnetically induced transparency," *Nature Commun.*, vol. 5, 2014, Art. no. 5753.